# Progress on the study of two photons speckles

Master's Thesis
Master of Experimental Physics
Thierry Kauffmann July 14, 2009

**Under the supervision of**
Ir. Wouter H. Peeters
Prof. Dr. Martin P. van Exter

Quantum Optics and Quantum Information
Leiden Institute of Physics (LION)
Leiden University

**Abstract**

This thesis is about the progresses brought to the two photon speckles experiment, after the work J.J.D Moerman achived [5]. What one calls a two photon speckle is the pattern of the coincidental clicks of two detectors in the far-field of a random phase plate (diffuser) shined by an entangled two photon field -in our experiment, this one is the two photon field coming Spontaneous Parametric Down-Converted coherent blue beam.

We inherited from Moerman equations and setup already done, as well as first scans and numbers, but no extensive studies of the speckle size.

We studied in great detail the two photon speckle size, and found out why the two photon speckles were a lot smaller than theory : the diffuser was not in the actual focus of the SPDC beam. After replacing the diffuser, we built a setup to be able to tune the number of excited modes in spatial entanglement by tuning the size of the pump beam continuously while keeping the focus right at its center. The setup is effective to tune the Schmidt Number from 30 to 1.5.

# Acknowledgements

It is quite obvious that I would like to thand everyone who let me work in here, on this project. The first step was administrative, and I am thankful to Reyer Jochemsen and Eric Eliel for the way they welcomed me (offering me a coffee, actually). Letting me visit all labrooms, talk with everyone about the current project and then letting me choose a project and a supervisor which I liked at the first sight is a good step done towards a fruitful internship. On this administrative part I would also like to thank Gerard Nienhuis for granting me credits for the first year of Master I did in France, it is not done in every faculty, and was therefore well appreciated (merci beaucoup Gérard pour le cours d'Optique Quantique, il était vraiment bien).

Thanks to this letting me choose, I had no worries about getting on well with Martin Van Exter, my supervisor. I was right not to worry. It is a pleasure to work with guies who have ideas (even more with the guies who have ideas the eyes wide shut). I also appreciated the enthusiasm, the always being positive. It is not so common not to like the early Monday morning meeting, that obliges you to get up at dawn after an exhausting week-end, and in which you'll have to skip your go saying "Sorry, nothing for this week, Maple bugged once more" or "For the third week in a row, I realigned the whole setup".

I did not choose to work actually with Wouter Peeters than with Martin, but I did not regret it. Having a conscencious PhD student to support you is precious. It is not so common that the supervisor is the one regretting the lack of contact between the student and the supervisor. You probably made me learn more than forty-seven loose supervisors all together ! I'll make my motto of your saying : "Science is not poetry : poetry is saying in a understandable way what everybody knows, science is just the contrary". You should be awarded a poetry prize for this sentence...

Thanks also to my fellow students, Filippo, Ziyu and Johannes (forget everything I said about German humor...). Without your jokes, I would definitely have been lost in this non-poetic scientific world. Daniele should be thanked too, for the feminine figure that, in the end, we all lack. And for her kindness too.

Thierry Kauffmann
Leiden, July 14, 2009

# Contents

# List of Figures

# Chapter 1

# Introduction

When many random-phased but coherent fields interfere, one calls it random [1]. Speckles have been present in science, since one thought to illuminatate a rough surface with a laser, and are used now in astronomy [2][3] and biology [4].

Speckles due to a coherent one photon field (like laser light), called to classical speckles, have been well studied [1]. In this thesis are considered the speckles created by a coherent two photon beam - even if there is no speckle in the intensity pattern, coincidences of photon detections show a speckle pattern.

In our case, the two photon beam is the infrared entangled two photon field generated by Spontaneous Parametric Down-Conversion (SPDC) of a blue laser beam. This two photon field is focussed on a random phase plate, called also diffuser, which is non-absorbing but presenting a random thickness (so adding a random phase). It is the contributions of this scattering that interfere on the far-field of the diffuser to create speckles.

The far field of the random phase plate will be measured by two detectors that can count single photons. What we call a coincidence is when two photons enter Detectors 1 and 2 -on the far field of the diffuser- simultaneously. The theory showing the speckle in the far-field coincidence count of the two photon field was already set before the work presented in this thesis - set by J.J.D. Moerman [5], as well as a setup and first measurements, which had not yet led to extensive study of the speckle sizes.

In Chapter 2 are going to be presented the "tools" we worked with, i.e the biphoton setup and equations describing these two photon speckles. In Chapter 3 is described the measurement programme we went for, and the results of the 70 scans we ran, and also the reason why the two photon speckles we had seen were not optimal.

Chapter 4 is all about the next step that we want to go for, what is reducing the number of modes involved in the two photon field - a short overview of the theory of reducing the number of modes, a experimental way of doing it and the first results are given.

# Chapter 2

# Setup and Theory of the two photon speckles experiment

Joining the group in September, I heritated from Hans, Wouter and Martin a working biphoton speckles generating setup, and theory which went with. This chapter, mainly borrowed to [5] and [6] will be there for the rest of the thesis to be understandable, and not to present my personal labour.

## 2.1 Setup

An overview of the setup for the biphoton experiment is given in Figure 2.1

The $\lambda_p = 413$ nm pump beam is coming from a Krypton ion gas laser (Coherent Innova 300), with a power of $200 \pm$ mW.

The pump beam is focussed on a 5 mm long periodically-poled $KTiOPO_4$ crystal (PPKTP) with $f = 1000$ mm lens A. The waist of the focus in the SPDC crystal is $w_{\mathrm{p}} = 170$ $\mu$m. A small fraction of this beam is converted in a $\lambda_0$ two photon beam, via Spontaneous Parametric Down-Conversion (SPDC). A GaP plate is place right after the PPKTP crystal so as to absord all the blue photons remaining.

A $f - 2f - f$ system is used to make an exact one-to-one image of the near field of the crystal on the diffuser plate, so as the beam is focussed on the diffuser ($f = 200$ mm). The diffuser plate has an opening angle of approximately $1^\circ$, and is placed so as the rough surface is towards the incident SPDC beam.

Behind the diffuser, a $f = 250$ mm lens is used in an $f - f$ system to make an image of the far field of the diffuser (Far Field 2). In between Lenses C and D, a 50-50 beam splitter is placed to split the photon pair in two outgoing directions. This beam splitter loses half the coincidence because there is only a $50\%$ probability that the photons of a pair choose two different paths through the beam splitter (both photons of a pair have to enter another detector to be counted as a coincidence).

The far field image (Far Field 2) is monitors with two detectors mounted on actuators, which can move in both tranverse directions. Each detector mode comprises of an $f = 8$ mm object lens and a single mode fiber. Both object lens, protected by a 5 nm wide 826 nm centered filters, are used to focus the incoming light into the fiber (with a mode field diameter of MFD $= 5.6$ $\mu$m).

The size of the detector modes in Far Field 2 is $\theta_D = 0.40$ mrad -low enough to see speckles which will be larger than $0.70$ mrad, see Section 3.3

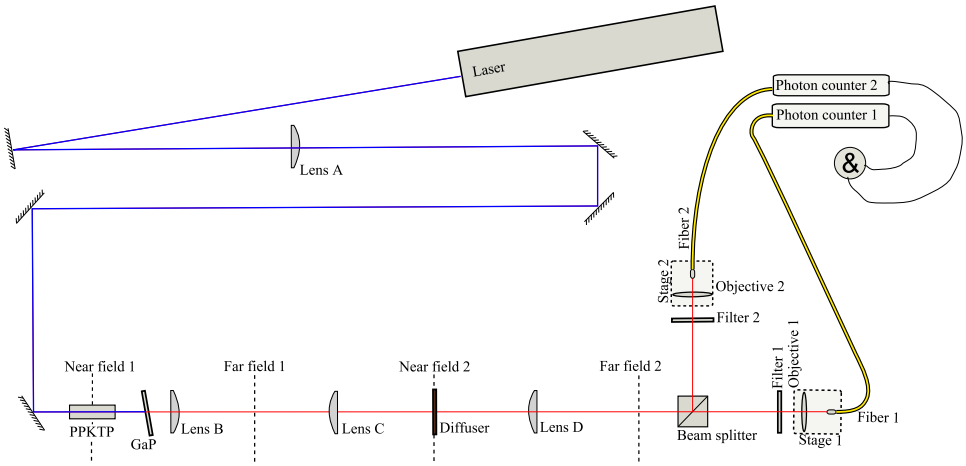


Figure 2.1: Schematic picture of the experimental setup for the biphoton speckle experiment. A beam from the laser is focussed onto a PPKTP crystal (Near Field 1) using lens A. Directly behind the crystal the remaining blue light is filtered out using a AR-coated wafer of GaP. A one-on-one near field (Near Field 2) image of the crystal is made onto a diffuser plate using lenses B and C. Behind the diffuser lens D makes a far field image (Far Field 2) of the diffuser plate on the detector modes. Both detector modes are separated by a beam splitter. The detector modes are composed of a fiber and an object lens that focusses the light on the fiber. Both detectors are indicated by the dotted areas denoted as Stage 1 and Stage 2. The fibers are connected to photon counters 1 and 2. Courtesy of J.J.D Moerman, reference [5] Figure 1

The two fibers are connected to single photon counters (SPCM-AQR). The electric pulses are then going to a fast AND gate that serves as a coincidence circuit with a specified gate time of $\tau_{\text{gate}} = 1.73$ ns. The coincidences counts are integrated over $\tau_{\text{int}} = 4$ s for each position of the detectors to get the average coincidence count rate.

One has also to consider accidental counts, which are not a manifestation of the biphoton field but just two uncorrelated photons that happen to enter the detector at the same time. It can be estimated by

$$R_{\text{acc}} = R_1 R_2 \tau_{\text{gate}} \tag{2.1}$$

where $R_1$ and $R_2$ are the single photon count in detector 1 and detector 2. The raw coincidences are corrected with these accidentals to obtain the corrected coincidence counts -accidental and corrected coincidence counts are about of the same order, so it is important to have this correction.

Equation 2.2 to Equation 2.5 are a recap of the numbers that will play an important role within Chapters 2 and 3.

$$L_{\text{cryst}} = 5.09 \text{ mm} \tag{2.2}$$
$$w_{\text{p}} = 170\ \mu\text{m} \tag{2.3}$$
$$\lambda_0 = 826 \text{ nm} \tag{2.4}$$
$$n_0 = 1.842 \tag{2.5}$$

## 2.2 Theory of the biphoton speckles

In this section will be presented an important result we relied on to process on biphoton speckles : the statistical shape of the spatial correlation function of the coincidence counts (handily also written $R_{\text{cc}}$).

The beam in the SPDC crystal is supposed to be Gaussian, focussed with a width $w_{\text{p}}$ -corresponding to a transverse intensity distribution

$$E_p(\boldsymbol{x}) = E_0 \exp\left(-\frac{\boldsymbol{x}^2}{{w_{\text{p}}}^2}\right) \tag{2.6}$$

It gives a biphoton field of the SPDC beam at the crystal center of [7]

$$A_{\text{SPDC}}(\boldsymbol{x}_1, \boldsymbol{x}_2) = A_0 \,.\, E_{\text{p}}\left(\frac{\boldsymbol{x}_1 + \boldsymbol{x}_2}{2}\right) \int \text{sinc}\left[\frac{\lambda_p L}{8\pi n_0}\boldsymbol{q}_-^2 + \phi\right] \exp\left[\frac{1}{2} i\,(\boldsymbol{x}_1 - \boldsymbol{x}_2)\cdot\boldsymbol{q}_-\right] d\boldsymbol{q}_- \,. \tag{2.7}$$

where $\boldsymbol{x}_1$ and $\boldsymbol{x}_2$ are the transverse position vectors for the two photons and the integration element $\boldsymbol{q}_-$ represents the difference in the far field wave vectors. The parameters that define the field are the size of the crystal $L$, the frequency of the pump $\lambda_p$ and the refractive index $n_0$ in the crystal for the low energy wavelength and the phase mismatch $\phi$, that we will consider null in Chapters 2 and 3.

Under a regime in which the pump is weakly focussed in the nonlinear crystal to generate many entangled spatial modes (Schmidt number $K \gg 1$, see Section 4.1), it gives a remarkable form to the SPDC beam [7] : $A$ can be separated into two functions that depend one of the sum of coordinates and the other on the difference of coordinates

$$A_{\text{SPDC}}(\boldsymbol{x}_1, \boldsymbol{x}_2) = A_0 E_p(\frac{\boldsymbol{x}_1 + \boldsymbol{x}_2}{2}) V(\boldsymbol{x}_1 - \boldsymbol{x}_2) \,, \tag{2.8}$$

where $E_p$ is the pump beam profile and $V$ the phase matching profile -in the near-field, the latter is much more compact than the first [8].

As we are using a type I geometry, the condition of weak-focussing is compulsory [6]. Given our geometry and the following approximation - valid as $\phi \approx 0$ [9]

$$\mathrm{sinc}[b\,\boldsymbol{q}_-^2] \approx \exp[-ab\,\boldsymbol{q}_-^2]\,, \tag{2.9}$$

with $a = 0.455$,

$$V(x) = \exp\left(-\frac{x^2}{w_-^2}\right) \tag{2.10}$$

$$w_- = \sqrt{\frac{a\lambda_p L}{\pi n_0}} \tag{2.11}$$

is called the phase matching parameter, which can be interpreted as the distance between the two photons of a photon pair.

The diffuser is placed in the near field image of the crystal. Directly behind the diffuser the field $A$ picks up a random phase based on the random functions $\phi(\boldsymbol{x_1})$ and $\phi(\boldsymbol{x_2})$ for both photons

$$A_d(\boldsymbol{x}_1, \boldsymbol{x}_2) = A_{\text{SPDC}}(\boldsymbol{x}_1, \boldsymbol{x}_2) \exp\left(i\boldsymbol{\phi}(\boldsymbol{x}_1) + i\boldsymbol{\phi}(\boldsymbol{x}_2)\right)\,. \tag{2.12}$$

This can be propagated to the far field [10]

$$A_{\text{FF}}(\boldsymbol{\theta}_1, \boldsymbol{\theta}_2) = \int\int A_d(\boldsymbol{x}_1', \boldsymbol{x}_2') \exp\left(\frac{-2i\pi f(\boldsymbol{\theta}_1 \cdot \boldsymbol{x}_1' + \boldsymbol{\theta}_2 \cdot \boldsymbol{x}_2')}{\lambda_0}\right) d\boldsymbol{x}_1' d\boldsymbol{x}_2'\,. \tag{2.13}$$

Actually, the coincidence count of the two detectors in the far field $R_{\text{cc}}(\boldsymbol{\theta}_1, \boldsymbol{\theta}_2)$ is proportional to $A_{\text{FF}}(\boldsymbol{\theta}_1, \boldsymbol{\theta}_2)$, just as the intensity is proportional to the square of the amplitude of the electric field. Let us choose the units so as

$$R_{\text{cc}}(\boldsymbol{\theta}_1, \boldsymbol{\theta}_2) = |A_{\text{FF}}(\boldsymbol{\theta}_1, \boldsymbol{\theta}_2)|^2 \tag{2.14}$$

That is why we can confound their two correlation function in what follows.

The key-function for this experiment is the fourth moment $\Gamma^{(4)}$ in the far field of the diffuser, defined by

$$\Gamma^{(4)}(\boldsymbol{\theta}_1, \boldsymbol{\theta}_2, \boldsymbol{\theta}_1', \boldsymbol{\theta}_2') = \langle R_{\text{cc}}(\boldsymbol{\theta}_1, \boldsymbol{\theta}_2) R_{\text{cc}}(\boldsymbol{\theta}_1', \boldsymbol{\theta}_2')\rangle_{\text{D}} \tag{2.15}$$

where $\langle\rangle_{\text{D}}$ means averaging over all realizations of the diffuser (or on all positions of a large diffuser). Here $\boldsymbol{\theta}_1$ and $\boldsymbol{\theta}_2$ are two-dimensional vectors with the angular position of detectors 1 and 2. The primed coordinates are also two-dimensional vectors for the positions of another pair of detectors 1 and 2. It will be useful to introduce new coordinates that represent the difference in position of the detector modes and their sum

$$\boldsymbol{\theta}_s \equiv \boldsymbol{\theta}_1 + \boldsymbol{\theta}_2 \tag{2.16}$$

$$\boldsymbol{\theta}_d \equiv \boldsymbol{\theta}_1 - \boldsymbol{\theta}_2 \tag{2.17}$$

Using the coordinates

$$\boldsymbol{\Sigma\theta}_s \equiv \left(\boldsymbol{\theta}_1{}' + \boldsymbol{\theta}_2{}'\right) + \left(\boldsymbol{\theta}_1 + \boldsymbol{\theta}_2\right) \tag{2.18}$$

$$\boldsymbol{\Delta\theta}_s \equiv \left(\boldsymbol{\theta}_1{}' - \boldsymbol{\theta}_2{}'\right) + \left(\boldsymbol{\theta}_1 - \boldsymbol{\theta}_2\right) \tag{2.19}$$

$$\boldsymbol{\Sigma\theta}_d \equiv \left(\boldsymbol{\theta}_1{}' + \boldsymbol{\theta}_2{}'\right) - \left(\boldsymbol{\theta}_1 + \boldsymbol{\theta}_2\right) \tag{2.20}$$

$$\boldsymbol{\Delta\theta}_d \equiv \left(\boldsymbol{\theta}_1{}' - \boldsymbol{\theta}_2{}'\right) - \left(\boldsymbol{\theta}_1 - \boldsymbol{\theta}_2\right) \tag{2.21}$$

$\Gamma^{(4)}$ can be expressed [6]

$$\Gamma^{(4)}(\boldsymbol{\theta}_1, \boldsymbol{\theta}_2, \boldsymbol{\theta}_1{}', \boldsymbol{\theta}_2{}') = f_{\text{shell}}(\boldsymbol{\Sigma\theta}_s, \boldsymbol{\Sigma\theta}_d) \times \left[1 + \exp\left(-\left(\frac{\Delta\boldsymbol{\theta}_s}{\theta_\text{p}}\right)^2\right) \exp\left(-\left(\frac{\Delta\boldsymbol{\theta}_d}{\theta_\text{d}}\right)^2\right)\right] \tag{2.22}$$

with the two angular widths having a similar expression

$$\theta_\text{p} = \frac{\pi\lambda_0}{w_\text{p}} \tag{2.23}$$

$$\theta_\text{d} = \frac{\lambda_0\pi}{w_-} \tag{2.24}$$

The shell function is supposed to depend on the opening angle of the diffuser and therefore be broader than the scan ranges [5], but in reality we suspect it being not so cutely wide. However, that is why a $1^\circ$ opening angle diffuser is used, in order that the shell function keeps flat, but the counts do not go too low.

# Chapter 3

# Proceeding to experiments

As written in Chapter 2, the setup and equations were waiting for me. But no proper experimental data was there to prove (or maybe discard) theory. Hans had run a scans, but he has not studied in great detail the speckles due to the compact $V(\boldsymbol{\theta}_x)$ (diff speckles). These were obviously not big enough compared to what theory predicted, and that is what we have studied extensively.

## 3.1 Measurement programme

So as to have systematic analyzes, we have set a strict measurement programme. The first issue has been to know which scans to run, in order to have the most relevant two photon speckles pictures without losing too much time. The easiest could have been to have a complete 4D scan, letting the two actuators scan both transverse directions. But unfortunately, a 2D $4000$ $\mu$m-diameter scan, with steps of $80$ $\mu$m was already taking a whole day. That is why we have had to imagine 2D scans which would tell the more possible about the two photon speckles. The more telling ones we have had are to the number of three. First "difference scans" (resp. "sum scans"), keeping $\boldsymbol{\theta}_\mathrm{s}$ (resp. $\boldsymbol{\theta}_\mathrm{d}$) constant - what means having in both cases $X_1$ and $Y_1$ as variables and setting the couplings $X_2 = -X_1$ (resp. $X_2 = X_1$) and $Y_2 = -Y_1$ (resp. $Y_2 = Y_1$). Then "X1X2 scans", taking $X_1$ and $X_2$ as variables and keeping $Y_1$ and $Y_2$ constant. $\boldsymbol{\theta}_\mathrm{d}$ kept constant along a diagonal, $\boldsymbol{\theta}_\mathrm{s}$ along the other, so these "X1X2 scans" would allow to acquire data on both sum and difference coordinates, depending on which diagonal we would project the scan on. Actually, to optimize the frame -save time-, the X1X2 scans axis have been rotated, so as a X1X2 scan would look like the others, being a square with $\boldsymbol{\theta}_\mathrm{d}$ and $\boldsymbol{\theta}_\mathrm{s}$ for axis. These various scans have been repeated with different spots on the LSD illuminated by the beam. There is one example of diff scan in Figure 3.3, of sum scan in Figure 3.4, of rotated X1X2 scan in Figure 3.5 and of non-rotated X1X2 scan in Figure 3.7.

Actually, a diff scan is equivalent to watching a scattered coherent pump beam $E_p(\boldsymbol{\theta}_s)$, whereas a diff scan is linked to the SPDC transport field $V(\boldsymbol{\theta}_s)$ (see Equations 2.8 and 2.22).

One could also have thought to monitoring $R_\mathrm{cc}$ when moving only one detector, and keeping the other one fixed. But as illustrated by Figure 3.1, it is almost equivalent to zoom twice on a sum scan. The reason for them presenting the same pattern is that even if a single detector moving will have equal $\Delta\boldsymbol{\theta}_d$ and $\Delta\boldsymbol{\theta}_s$, because in Equation 2.22 $\theta_\mathrm{d} \gg \theta_\mathrm{p}$, the effect of $\Delta\boldsymbol{\theta}_d$ will hardly be seen compared to the ones of $\Delta\boldsymbol{\theta}_s$. The factor 2 in the

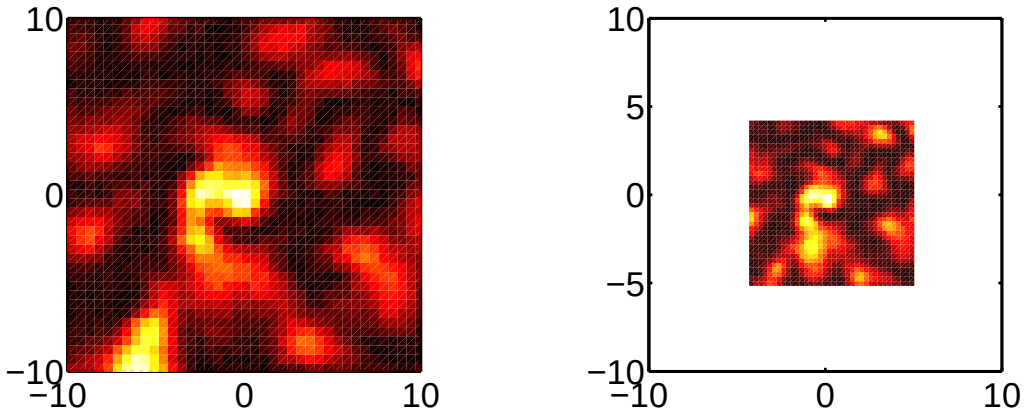


Figure 3.1: On the left is the $R_{cc}$ pattern of the single detector scan (i.e. $\boldsymbol{x}_{\text{detect1}}$ was moving and $\boldsymbol{x}_{\text{detect2}}$ fixed, and on the right the $R_{cc}$ pattern of the sum scan , both centered on the same spot. The lab-ID of these two experiments are 060701moerman06fixed and 060702moerman02fixed respectively

zooming is only that in a sum scan

$$\Delta\boldsymbol{\theta}_s = 2\Delta\boldsymbol{\theta}_1 \tag{3.1}$$

So,as the finite size of the beam is a limitation to our statistics, better have a sum scan with a twice lower resolution than a single detector scan, which would give four times less information for the same scan range.

The reason why only the two photon correlations have been scanned is that as the single photons of a biphoton field are incoherent, the output of one single detector ($R_1$ or $R_2$) gives no interesting feature : you see only small fluctuations and impurities added to the Gaussian profile of the beam (the normalized variance will be low, see Equation 4.4). In Figure 3.2 is given an arbitrary profile of the first detector (the one of a scan named 081015kauffmann-run3).

Actually, for now, information is given only by the width of $\Gamma^{(4)} - 1$ (which is supposed to be Gaussian, see Equation 2.22).

## 3.2 Procedure to analyze the scans

### 3.2.1 Quantum Efficiency or $R_{cc}$

Previous section describes how $R_{cc}$ of different scans was recorded. But it is also important to determine whether it is more relevant to study the correlations of $R_{cc}$, or of the so called Quantum Efficiency (also written Q.E, or $\eta$), defined as

$$\eta \equiv \frac{R_{cc}}{\sqrt{R_1}\sqrt{R_2}} \tag{3.2}$$

The argument in favor of $R_{cc}$ is very simple : if its correlation function can be (statistically) predicted as in Equation 2.22, the theory for the Quantum Efficiency is much wilder, because of the correcting with $R_1$ and $R_2$ in its definition 3.2.

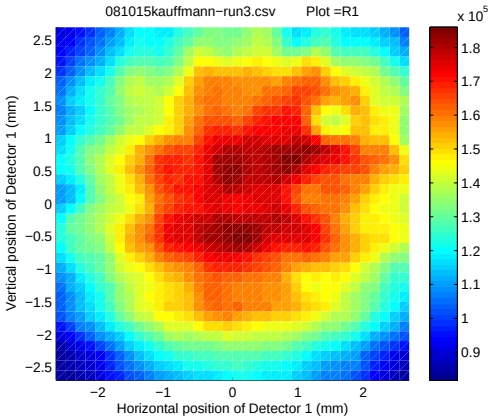


Figure 3.2: $R_1$ pattern of the scan named 081015kauffmann-run3

But $\eta$ has the advantage of removing possible fluctuations or aberrations present in the single counts. As a whole $R_{cc}$ pattern took hours to be shot, there could be slight drifting from the laser, leading to intensity and single count drops.

Another advantage of $\eta$ is to theoretically allow to work with an infinite scan range. Experimentally, one cannot rely on too low single counts, but $\eta$ had always a larger reliable zone.

To test whether there is a significant difference in the speckle sizes of $\eta$ and $R_{cc}$ we have extracted the speckles sizes in both ways for three experiments : the $1\ s$ integration time, $150\ \mu$m resolution, $5400\ \mu$m diameter diff scan named 081021kauffmann-run1fixed in Figure 3.3, the 1 s integration time, $75\ \mu$m resolution, $5400\ \mu$m diameter sum scan named 081022kauffmann-run1fixed in Figure 3.4 and the 1 s integration time, $80\ \mu$m resolution, $8000\ \mu$m diameter X1X2 scan named 081026kauffmann-run1 in Figure 3.5.

In Figure 3.3 scan $R_1$ counts keeps almost constant where the speckle is, where as it is presents a contrast of 2 in Figure 3.4 and a contrast of 10 in Figure 3.5, and one can notice that the bigger the $R_1$ contrast, the more different $R_{cc}$ and $\eta$ patterns are one from the other. But we can see in these three examples that there is no easy rule on what is the difference between the size of the speckles for the two patterns. We do not have the number for both ways for all experiments, but made as if the speckles should have the same size on average.

To conclude, for "everyday experiments" we have scrutinized the Quantum Efficiency for its being smoother, but for measuring publishable numbers, $R_{cc}$ has been preferred.

### 3.2.2 Discussion on the calculation of the correlation matrix

Once having chosen $R_{cc}$ or $\eta$, one step left towards the autocorrelation width is to decide how to calculate this autocorrelation function $\Gamma^{(4)}$.

Actually, to calculate $\Gamma^{(4)}$, we have used two Matlab routines. The first one, named ComputeCorrelationMatrix, fills the plane with copies of the $\eta$ matrix and then calculates the correlation matrix (filling the plane avoids the boundary issues), and then AverageAroundCenter outputted rotational, vertical and horizontal 1D average of the 2D $\eta$ pattern.

The question raised is whether it is relevant to first surround the $R_{cc}$ pattern with a constant field before the repeating of the fast Fourier transform of ComputeCorrelationMatrix,

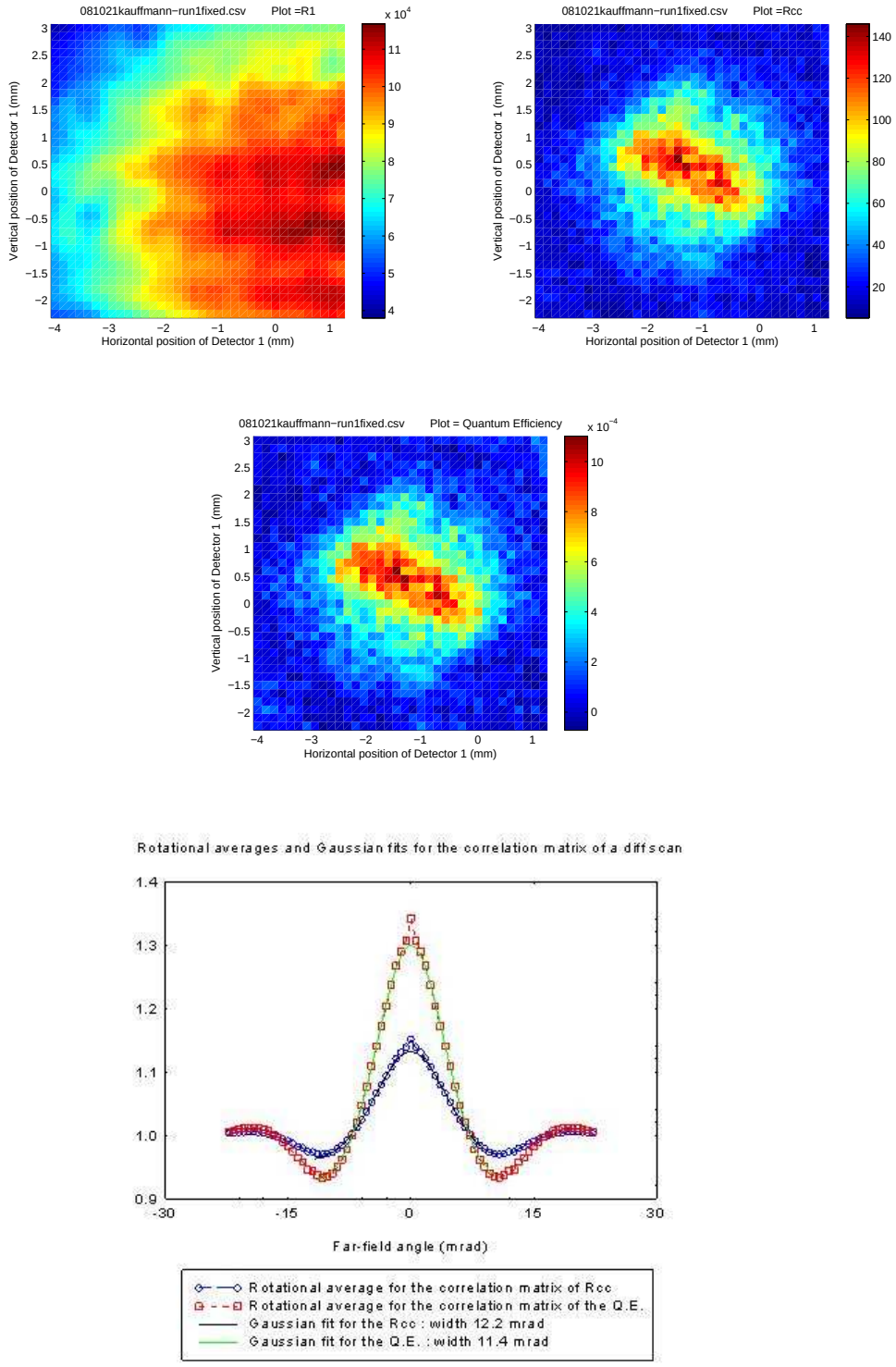


Figure 3.3: All graphes concern the diff-scan named 081021kauffmann-run1fixed : on the top left is the $R_1$ pattern, on the top right $R_{\mathrm{cc}}$, on the bottom left $\eta$. On the bottom right is a graph showing Gaussian fits of the central peaks of the rotational averages of the correlation matrices of the $R_{\mathrm{cc}}$ and $\eta$ patterns of this very scan.

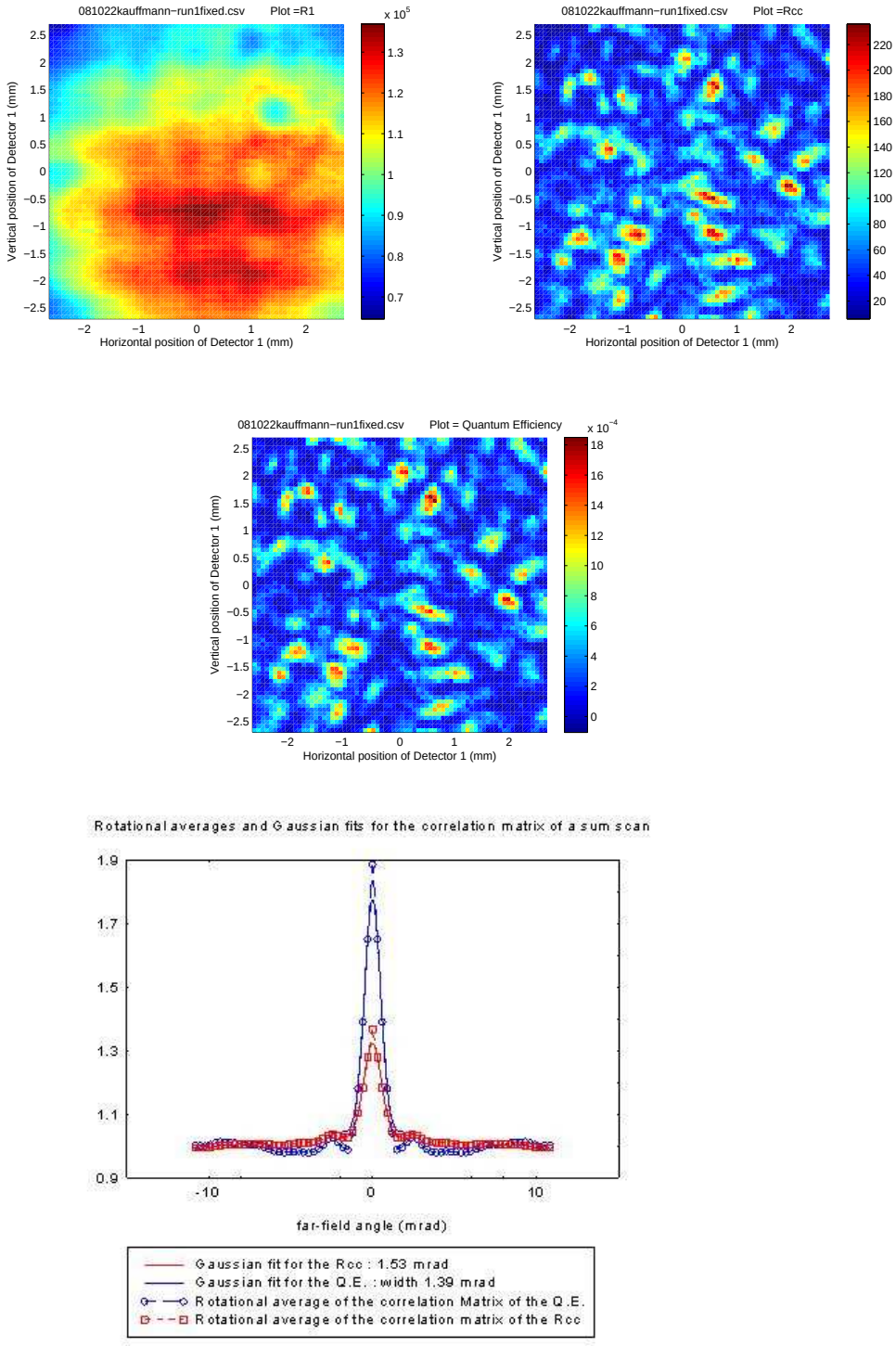


Figure 3.4: All graphes concern the sum-scan named 081022kauffmann-run1fixed : on the top left is the $R_1$ pattern, on the top right $R_{\text{cc}}$, on the bottom left $\eta$. On the bottom right is a graph showing Gaussian fits of the central peaks of the rotational averages of the correlation matrices of the $R_{\text{cc}}$ and $\eta$ patterns of this very scan.

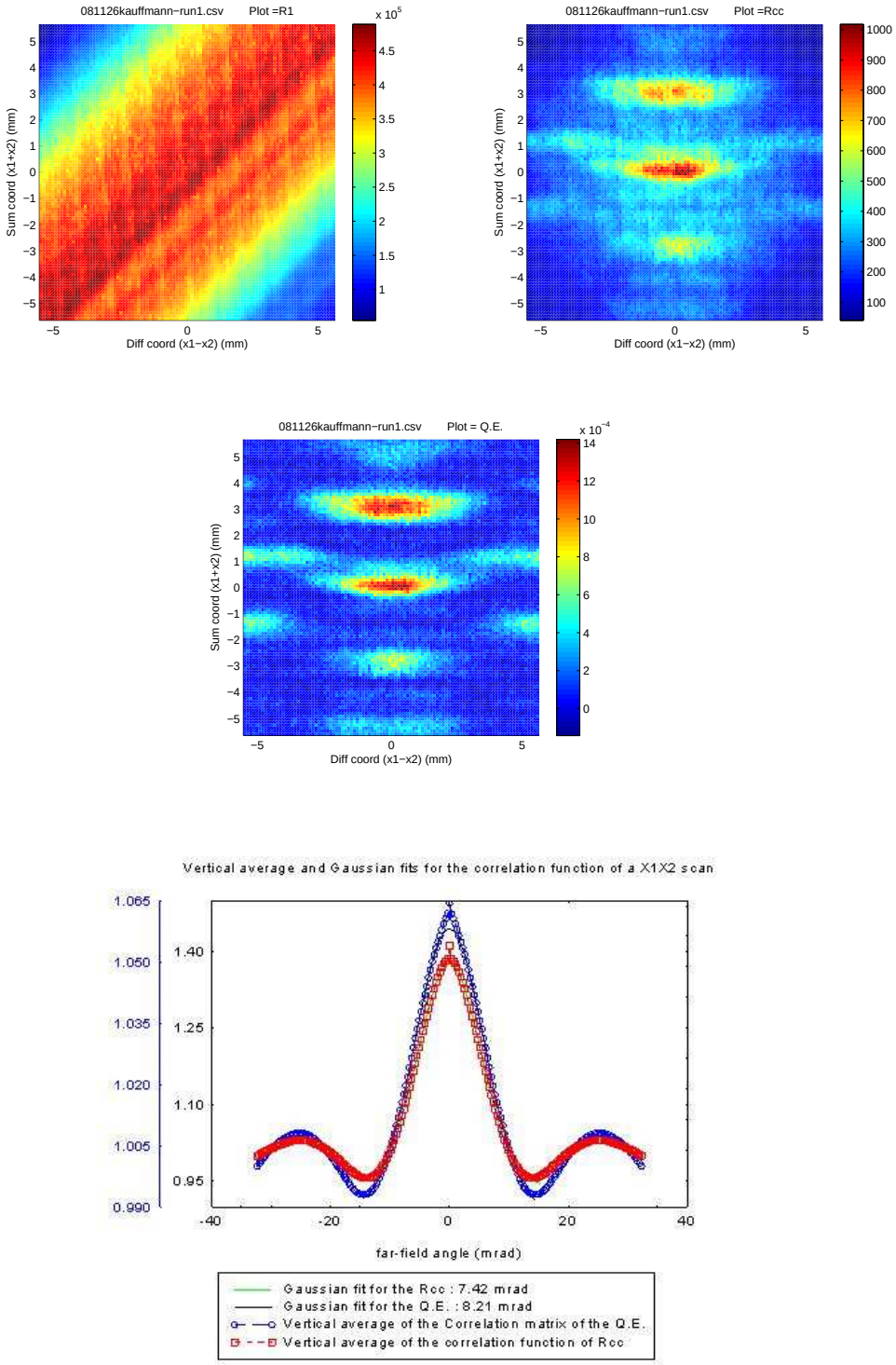


Figure 3.5: All graphes concern the X1X2-scan named 081126kauffmann-run1 : on the top left is the $R_1$ pattern, on the top right $R_{\text{cc}}$, on the bottom left $\eta$. On the bottom right is a graph showing Gaussian fits of the central peaks of the rotational averages of the correlation matrices of the $R_{\text{cc}}$ and $\eta$ patterns of this very scan.

and then which constant to go for. The reason for imagining extending the original pattern with a constant is to avoid that a speckle to the left of the scan is merging together with one on the right when the repeating takes place.

Two values for the constant look logical : either black suited more $R_{\mathrm{cc}}$, as it goes down to 0 at infinity (the beam has obviously a finite size), or take the average value of the pattern was more for $\eta$, as it should never vanish, and also to avoid too brutal a gap between the actual scan and its fake surrounding.

In Figure 3.6 is given the three possible $\eta$ patterns we can build, and then the three rotational averages of the three possible correlation that come out these three first $\eta$ pattern, for a diff scan named 081024kauffmann-run1. One can see on this scan that the speckle size is the same on the $\eta$ extended with black and with average, but are $15\ \%$larger for the "repeated" $\eta$.

We have calculated the widths of the autocorrelation matrices (by using a computed Gaussian fit) with repeated and average-extended $\eta$ patterns of up to 60 scans. The ratio between the two values of the fitted $\theta_{\mathrm{d}}$ of Equation 2.22 (what is actually difference speckles size),

$$\frac{\theta_{\mathrm{d_{repeated}}}}{\theta_{\mathrm{d_{extended}}}} = 1.11 \pm 0.11, \tag{3.3}$$

whereas the same ratio for the values of the $\theta_{\mathrm{p}}$ (sum speckles size) is

$$\frac{\theta_{\mathrm{p_{repeated}}}}{\theta_{\mathrm{p_{extended}}}} = 1 \pm 0.04. \tag{3.4}$$

We can conclude that, as the "sum coordinate" speckles are small, their border effect is negligible, so $\theta_{\mathrm{p}}$ is not dependent on the method we use. On the other hand, difference coordinate speckles are much larger and a merging will have a bigger effect, that is why the value calculated with a repeated $\eta$ is somehow ten percent bigger than the one obtained with an extended $\eta$ - but may also be a little lower is some experiments, as some scans show particular features.

## 3.3 Experimental results

In this section will be presented the extensive experimental results of the first wave of scans, ran between October and December 2008, with experimental numbers given from Equation 2.2 to 2.5.

Theory predicts a pump angle of $\theta_{\mathrm{p}} = 0.77$ mrad . We also obtain $\theta_{\mathrm{d}} = 14.5$ mrad, what corresponds to a Fourier-related near-field size $w_{-} = 18.1\ \mu$m.

The output of this extensive study is mainly two measured numbers (coming from Equations 2.23 and 2.23) : $\theta_{\mathrm{p}} = 0.71$ mrad $\pm$ 0.09 mrad and $\theta_{\mathrm{d}} = 3.4$ mrad $\pm$ 1.25 mrad.

It is striking on how, if the measurements were almost in agreement with theory for the sum speckles, the diff speckles we measured were on average more than 4 times too smaller than predicted !

It can be explained by two major ideas.

The first one is that they should be approximately as big as the scan range (limited by mechanical issues and also by the size of the diffracted cone of the diffusor), so they may be "cut". But this does not explain so big a non-sticking to theory.

The major reason is that if the LSD is not precisely positioned in the near-field of the crystal, the $V(\boldsymbol{\theta}_d)$ profile may present too big a width, and therefore induce smaller

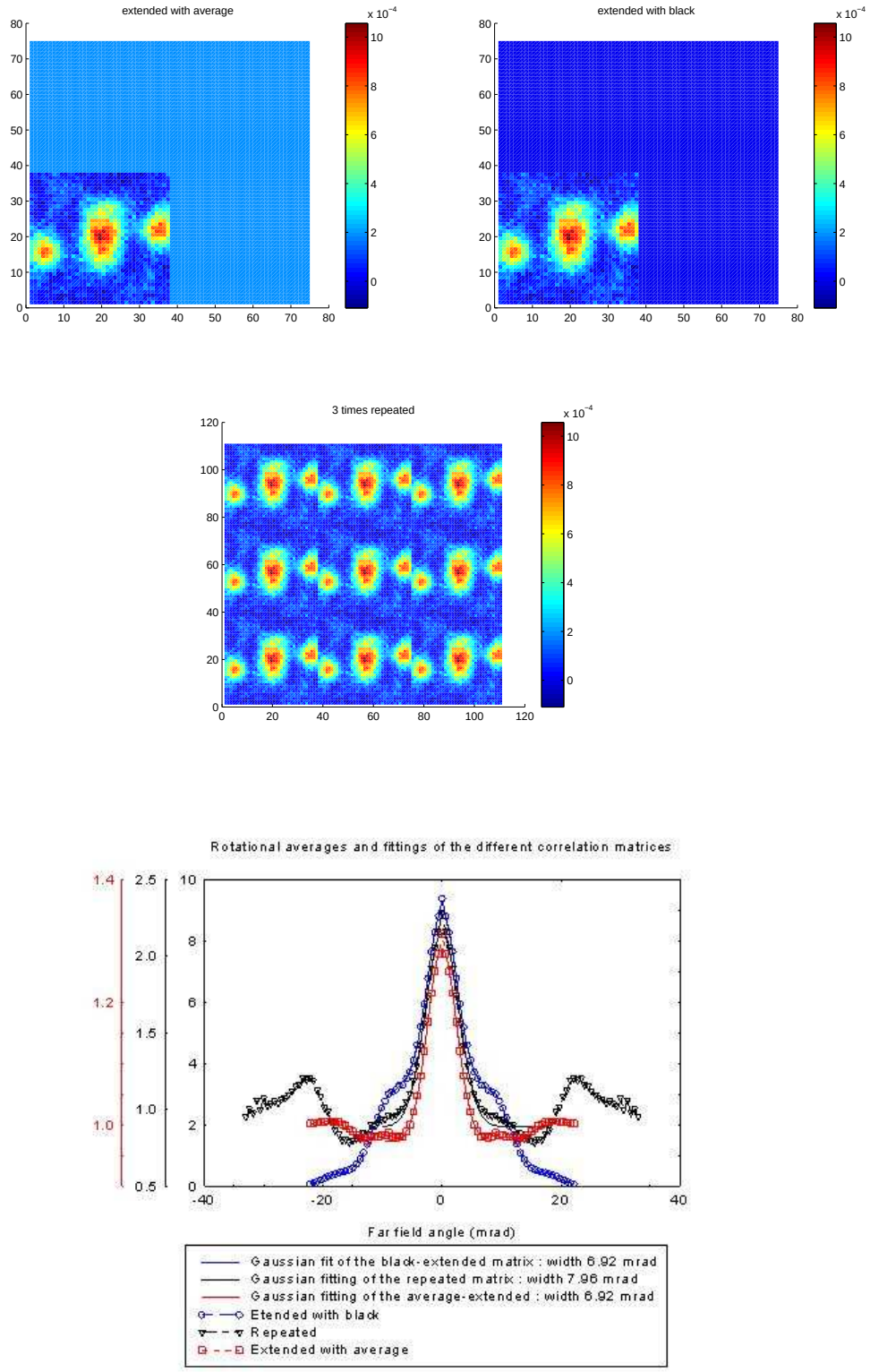


Figure 3.6: All graphes concern the diff-scan named 081024kauffmann-run1 : on the top left is the $\eta$ pattern extended with average, on the top right it is extended with black, on the bottom left it is "3-times repeated". On the bottom right is a graph showing Gaussian fits of the central peak of the rotational averages of the correlation matrices of these three types of $\eta$.

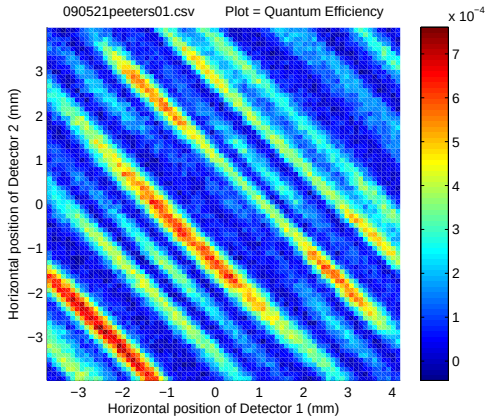


Figure 3.7: $\eta$ pattern of the scan named 090521peeters01, which presents a lot larger diff speckles. Courtesy of W. H. Peeters for the experiment data.

speckles. This was likelier realizing that, as $w_- = 18.1\ \mu$m, the Rayleigh range of this profile is $1.2$ mm.

Since this issue was tackled, diff speckles show the right size - in Figure 3.7 is given an example of "new" scan in which one can see much larger diff speckles.

A rapid calculation shows that on the first wave of experiments,

$$\overline{\theta_{\mathrm{dexp}}} = \frac{\theta_{\mathrm{dtheory}}}{4.26} \tag{3.5}$$

Assuming this difference comes all from the mispositioning of the diffusor, the width of $V(\boldsymbol{\theta}_d)$ in the diffusor was equal to $4.26\ w_-$, what implies, thanks to Gaussian beam properties, if $z$ is the mispositioning value (in meters),

$$w_- \sqrt{\left(1 + \left(\frac{z}{z_{\mathrm{R}}}\right)\right)} = 4.26\ w_-\ . \tag{3.6}$$

The number that we can extract is

$$z = 5\ \mathrm{mm}\ . \tag{3.7}$$

Having a low number for the estimated displacement justifies the hypothesis of mispositioning, considering that the diffuser was placed so as to be withing a pump Rayleigh range (which is larger than $20\ \mathrm{cm}$).

One can also notice that $\theta_{\mathrm{p}}$ is much more stable over the different positions on the LSD than $\theta_{\mathrm{d}}$, even if there is six times more measurements of the latter (ten compared to sixty). We can interpret this fact by the fact that as $\theta_{\mathrm{p_{exp}}} = 4.8\ \theta_{\mathrm{p_{exp}}}$, sum speckles are $4.8^2 = 23$ times more numerous than the difference speckles within a scan of the same range. So that could be a first explanation to why even with 6 times more data, the variance on the $\theta_{\mathrm{d}}$ measured was bigger than the one on the $\theta_{\mathrm{p}}$ - but actually, this is only partial, as because with a statistical, $23/6 = 4$ more sum speckles should bring a sum variance only twice as small as the difference variance.

A counter-effect was that, even if we would lower the resolution for a sum scan (step size down to $75\ \mu$m), it was not 5 times as low as the resolution we have used for diff scans

(which would oscillate between $100$ $\mu$m and $150$ $\mu$m). So the sum speckles have been less precisely spotted, and the variance has been raised by this effect.

# Chapter 4

# Reducing the mode numbers

Now that we have a better comprehension of the two photon speckles in the regime in which the SPDC beam can be factorized 2.8 and comprises many excited mode, we are looking forward to seing what differences a lower number of excited modes would bring on the two photon speckles experiment. We are suspecting that a low number of excited mode would induce less averaging in the far-field. And we are also excited by seing how the SPDC beam on itself looks like in a non-factorized regime.

## 4.1 Schmidt Number

### 4.1.1 Definition and first results

The Schmidt number is a well known number to characterize the spatial entanglement of a biphoton field such as ours - one can call it "number of modes", even if this denomination is looser.

It follows the Schmidt decomposition of the input state

$$A(\boldsymbol{x}_1, \boldsymbol{x}_2) = \sum_\mu \sqrt{\lambda_\mu} u_\mu(\boldsymbol{x}_1) v_\mu(\boldsymbol{x}_2)\,, \tag{4.1}$$

with eigenvalues $\lambda_\mu$ and normalized eigenstates $u_\mu$ and $v_\mu$.

The Schmidt number is the defined as

$$K \equiv \frac{\left(\sum_\mu \lambda_\mu\right)^2}{\sum_\mu \lambda_\mu^2} \tag{4.2}$$

what is, if $A$ is normalized,

$$K = \frac{1}{\sum_\mu \lambda_\mu^2}\,. \tag{4.3}$$

If $N$ is the number of excited modes, $K$ will go from $N$ for a fully entangled field (flat distribution over all the modes) to 1 for a pure state (all photons in one single mode).

For the usual experiments using spontaneous parametric conversion, $K \gg 1$ -Henrique Pires has created an rather precise (less than $10$ % error) algorithm named SchmidtNumberAuto [11] showing that in our standard setup, with a $5$ mm long crystal, a pump beam waist of $170$ $\mu$m and a null phase mismatch, $K = 52$.

One very interesting effect of the Schmidt Number on the two photon speckles experiment is that the fine structure of the single and coincidence counts rates have a normalized variance equal to [6][12]

$$\mathrm{Var}(R_{1,2}) \equiv \frac{\left\langle R_{1,2}^2 \right\rangle_D}{\langle R_{1,2} \rangle_D^2} - 1 = \frac{1}{K} \tag{4.4}$$

$$\mathrm{Var}(R_{\mathrm{cc}}) \equiv \frac{\left\langle R_{\mathrm{cc}}^2 \right\rangle_D}{\langle R_{\mathrm{cc}} \rangle_D^2} - 1 = \frac{K+2}{K} \tag{4.5}$$

One can see that with these two equations that a many-modes field will have no local fluctuation on the single count rate ($\mathrm{Var}(R_{1,2}) \approx 0$) (Figure 3.2 gives an example) but fully developed two-photon speckles. Please notice that this $K \gg 1$ was the regime in use in all results of previous sections.

The common explanation for these results is that the one photon field of a SPDC field is incoherent, but the two photon field in itself is coherent.

On the other part of the scale, a single-mode field will show a one photon field which is also coherent, as seen in the result $\mathrm{Var}(R_{1,2}) = 1$. As $R_{\mathrm{cc}}(\boldsymbol{q}_1, \boldsymbol{q}_2) = R_1(\boldsymbol{q}_1) R_2(\boldsymbol{q}_2)$ , in this case one can retrieve the result $\mathrm{Var}(R_{\mathrm{cc}}) = 3$.

Before starting to observe these different speckles, a way to vary the Schmidt number between 30 and as low as possible was needed.

### 4.1.2 How to create a low Schmidt number field ?

There are several parameters coming into account into the Schmidt Number. The SPDC crystal length, the pump wavelength, the refractive index of the crystal are part of these [11], but are, if possible, inconvenient to tune continuously.

The phase mismatch plays also a role into the value of the Schmidt Number. Actually, it comes out from SchmidtNumberAuto that the minimum for the Schmidt Number is very close to a null phase mismatch. That is why we took $\phi \approx 0$ in our setup.

The very parameter reasonably easy to tune is $w_{\mathrm{p}}$, the pump beam waist in the crystal -in the center of the crystal is more precise, as for $w_{\mathrm{p}} = 30$ $\mu$m, the Rayleigh range $z_{\mathrm{R}}$ goes down to 7 mm, to be compared to the 20 mm length of the SPDC crystal we went for.

Based on SchmidtNumberAuto, we have computed the curve given in Figure 4.1 to know what range $w_{\mathrm{p}}$ should sweep.

As you can see in Figure 4.1, the answer is that, with a 20 mm long crystal and a null phase mismatch (which corresponds to a temperature of the crystal of $60.4°\mathrm{C}$), to have a Schmidt Number varying from the minimum ($K = 1.46$) to 30, $w_p$ has to sweep all values from 30 $\mu$m to 260 $\mu$m.

So, having this idea, all what was left was to find a way to build what we could call a "fixed-focus telescope".

## 4.2 Fixed-focus telescope theoretical setup

To achieve the fixed-focus telescope, we have had the idea to combine a few lenses, two of them being mounted on translating stages.

The restrictions we have fixed to ourselves to construct the setup that could be implemented on the biphoton setup were :

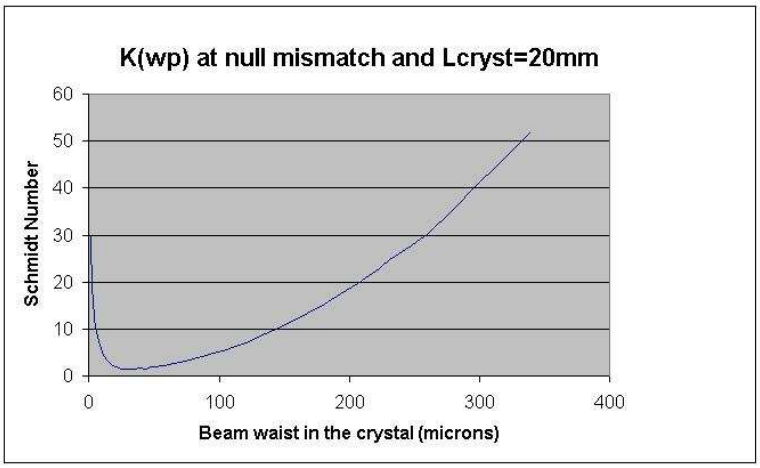


Figure 4.1: A computed curve giving a good approximation of the Schmidt Number in function of the (focussed) beam waist in the crystal, assuming a null phase mismatch and a 20 mm long crystal

- To have the beam varying from $w_{\mathrm{p}} = 30$ $\mu$m to $w_{\mathrm{p}} = 240$ $\mu$m
- To keep the beam focussed within a Rayleigh range of the center of the crystal
- To have not to move the lenses of more than the $40$ mm of the translating stage
- To have all intermediate foci not larger than $10$ $\mu$m, so as to avoid aberrations
- To keep all beams on lenses smaller than $1$ mm, so as to avoid spherical aberrations
- To keep the blur ring due to spherical aberrations smaller than $10\%$ of the beam's foci
- To keep this separate setup being a future add-on to the biphoton setup (as seen in Figure 2.1

An overview of the setup is given in Figure 4.3.

The laser input of the fixed-focus telescope setup was $2.4$ mW diverted from the biphoton setup laser, via a wedge and a single mode fiber (MDF $\approx 2.6$ $\mu$m, reference Thorlabs PM-S405-HP). A first duty was to transform a very divergent beam -1.3 $\mu$m at the output of the fiber- into something which looks like the laser beam of the biphoton setup seen in Figure 2.1 -1 mm broad almost collimated beam in between Lenses 1 and 2 in Figure 4.3. To calculate how turning the input fiber beam into to $1$ mm collimated beam, we have used a Maple computation sheet named "Calculation of the Input.mws", and it was quite obvious that a first lens which would suit would be around $f = 10.8$ mm, from an easy calculation of divergence. However, a Maple sheet was necessary to know were to place the two first lenses, because we had to go for a $f = 11$ mm lens instead of a $f = 10.8$ mm, for reason of availability.

To build the main part of the fixed-focus telescope, we have used another Maple sheet named "Fixed-focus-telescope Computation.mws". The two computation sheets use the

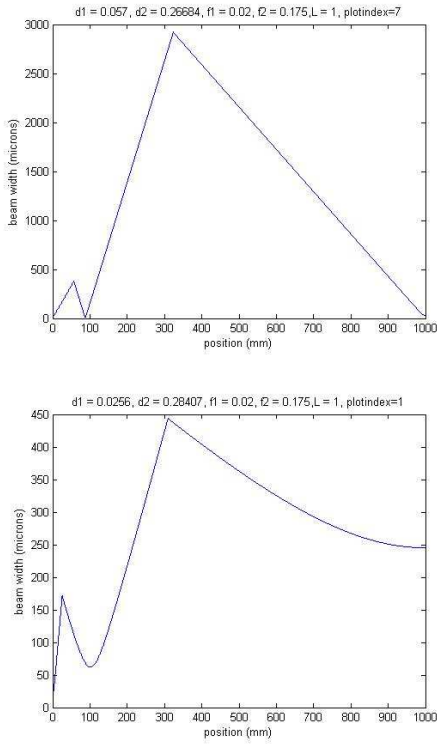


Figure 4.2: On the top is the beam profile between first intermediate focus ($w_1$) and PPKTP crystal ($w_\mathrm{p}$) for the regime $w_\mathrm{p} = 30$ $\mu$m, and on the bottom is the same profile for $w_\mathrm{p} = 250$ $\mu$m.

ABCD matrices theory, so as it is easy to keep the only solutions which have a focus at the center of the crystal.

The tricky part of the computation was to find out the right lenses strengths. Too strong a lens, too small would be the intermediate foci. Too weak a one placed on a translating stage, too short the translating stage would be to tune all $w_\mathrm{p}$ from 30 to 240 $\mu$m. A little feeling of Optics, and several tests and tries were required.

In Figure 4.2 are given the two beam profiles (after the first focus, as the beginning of the beam is not varying) under the regimes $w_\mathrm{p} = 30$ $\mu$m and $w_\mathrm{p} = 250$ $\mu$m.

All references to lenses used can be found in Figure 4.4.

The solution chosen for turning the input fiber beam into a collimated 1 mm beam was to place the 11 mm focal-length aspherical Lens 1 at 10.8 mm of the fiber output, then the 150 mm biconvex Lens 2 98.6 mm further.

Then we have been for two lenses mounted on 40 mm long translating stages, so as to be able to change beam size without changing the focus position. The first one, named Lens 3, was a 20 mm biconvex lens, positioned from 325.6 to 357 mm from the fiber output, whereas the Lens 4 was a 175 mm biconvex lens, positioned from 605 to 625 mm from the fiber. The center of the PPKTP crystal was positioned $125,5$ cm after the output of the fiber. In between the last lens and the PPKTP crystal, a flip mirror was placed to let us monitor the crystal with the Spiricon Camera (the distance from the flip mirror to

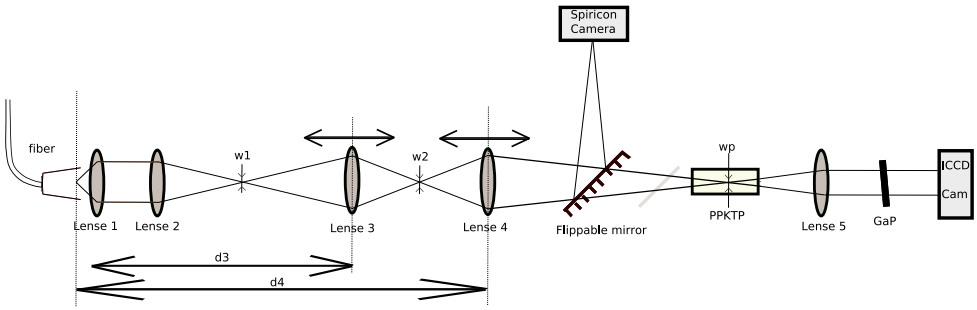


Figure 4.3: Overview of the setup of the fixed-focus setup. The key-role is played by lenses 3 and 4, as they are mounted on translating stages. In the far-field of the crystal is placed an Intensified CCD so as to see the SPDC-generated two photon field

the Spiricon Camera being the same as from the mirror to the center of the crystal). After the PPKTP crystal, a 200 mm biconvex lens and an Intensified CCD camera were placed in a f-f configuration with respect to the crystal so as the Intensified CCD would be in the far-field of the crystal. A GaP wafer is placed in between the crystal and the Intensified CCD camera so as to absorb all blue photons remaining after the SPDC process.

A theoretical curve giving the positions at which one should position Lenses 3 and 4 for a wanted $w_{\mathrm{p}}$ is given in the down curve of Figure 4.7.

A table of important numbers for this experiment is given in Figure 4.4.

## 4.3 On the table

After having theoretical numbers, we have tested them on the optical table. Facing numerous difficulties listed in Subsection 4.3.1, we could have results given in Subsections 4.3.2 and 4.3.3.

### 4.3.1 Deformations of the beam

The beam in the crystal have often showed severe deformations to what should be Gaussian. As the beam coming out the fiber was Gaussian, it means the beam faced deformations during the setup. In Figure 4.5 are given the Spiricon print screens of a solution to the problem, with a value of $w_{\mathrm{p}} = 100$ $\mu$m, 15 cm in front of the focus, at the focus and 15 cm after the focus (no crystal is in between, as the Spiricon was in another path than the crystal, thanks to a flip mirror).

One reason for this distortion is the poor quality of the density filters we used (a two density-filters wheels back to back, which could behave as a slight Fabry-Pérot interferometer), but it is not the only one at all, as even with single good-quality filters, some aberrations were still present.

Another major reason is aberrations due to lenses. If in Figure 4.4 one can see that, if correctly manufactured, Lenses 2, 3 and 4 should not bring aberrations, the blur ring due to Lens 1 may be blurring the beam in a significant manner, even if blur ring size given in

| Number | Tight focus regime | Loose focus regime |
|---|---|---|
| L1 | f=11 mm, aspheric, A397TM-A | 11 mm |
| f2 (Lens 2 strenght) | f=150 mm, biconvex, LB1437-A | 150 mm |
| f3 (Lens 3 strenght) | f=20, mm biconvex, LB1450-A | 20 mm |
| f4 (Lens 4 strenght) | f=175 mm, biconvex, LB1294-A | 175 mm |
| Distance fiber-crystal | 1.3 m | 1.3 m |
| Schmidt Number | 1.45 | 30 |
| b.sigma | 1.19 | 0.148 |
| d3 (distance fiber-Lens 3) | 35.7 cm | 32.56 cm |
| d4 (distance fiber-Lens 4) | 62.38 cm | 60.97 cm |
| w1 (first focus waist) | 19.7 micron | 19.7 micron |
| w2 (second focus waist) | 10.6 micron | 62 micron |
| wp(crystalt focus waist) | 30 micron | 246 micron |
| beam size in L1 | 903 micron | 903 micron |
| beam size in L2 | 1000 micron | 1000 micron |
| beam size in L3 | 380 micron | 170 micron |
| beam size in L4 | 2900 micron | 440 micron |
| Blur ring due to L1 | 3.26 micron | 3.26 micron |
| Blur ring due to L2 | 0.02 micron | 0.02 micron |
| Blur ring due to L3 | 0.07 micron | 0.007 micron |
| Blur ring due to L4 | 0.43 micron | 0.001 micron |

Figure 4.4: Overview of the setup of the fixed-focus setup important numbers. They are given for the two extreme $w_{\mathrm{p}} = 30$ $\mu$m and $w_{\mathrm{p}} = 248$ $\mu$m regimes. The calculation for the size of the blur ring due to lenses aberrations of lenses is given by OFR's $w_{\mathrm{blur}} = K \cdot f \cdot NA^3$, with $K = 0.067$ for a refraction index of $n = 1.5$. Blur ring size due to first lens is calculated for a biconvex lens, whereas Lens 1 was aspherical. So $w_{\mathrm{blur1}}$ is overestimated in this table.

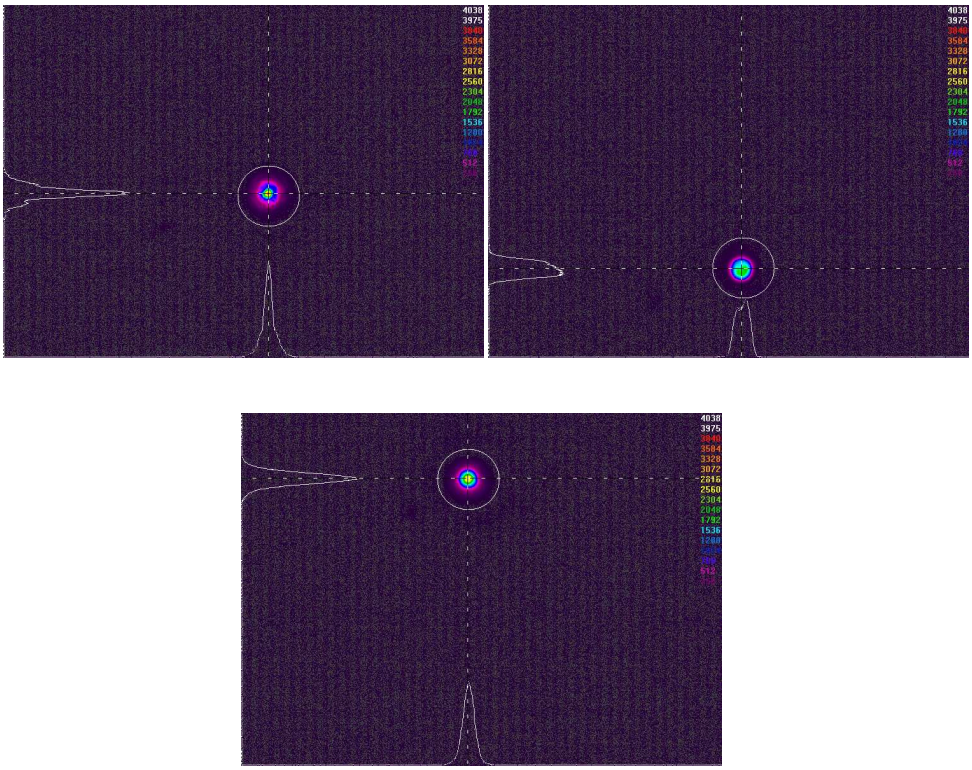

Figure 4.5: On the top left is the $w_{\mathrm{p}} = 100\ \mu\mathrm{m}$ $15\ \mathrm{cm}$ in front of the focus, on the top right is the same beam at the focus and on the bottom is the same beam $15\ \mathrm{cm}$ after the focus.

4.4 is overestimated. Actually, this number was calculated after all theoretical predicting was done, as the computations were done for the add-on to the biphoton setup, and not for the part to transform the input beam into a 1 mm collimated bean.

Fortunately, Lens 1 will no be present in the biphoton setup (Figure 2.1). Still, we suspect aberrations due to misalignment to occur.

A first tough gate was the $f = 11$ mm Lens 1, which had a diameter not so much larger than the beam's one. This one could bring easily aberrations, if the beam was not rigorously aligned with the center of the lens. By the time it was positioned, the beam did not present aberrations, but it may have happened that it was banged, or that the fiber output slightly drifted (due to mechanical reason).

But the main reason for this misalignment problems is probably Lens3, the $f = 20$ mm lens placed on a translating stage. This lens is indeed a strong one, and, because it being translated, needed that the axis of the translating stage was very parallel to the beam, and required also that the beam was very horizontal (less than 10 mrad of vertical angle). This lens was positioned as carefully as possible, superposing the beams with and without the lens being placed on a one meter far away screen -the longest distance possible with $2.4\ \mathrm{mW}$ of power because of the large divergence of the beam without the second lens. We would advise for the next time this setup is used to have the screen more than one meter far away, with a more power so as to see the divergent beam.

But fortunately aberrations were almost non existing on the tight foci regime, which is the one we wanted to study extensively. That is why the measurements we have taken are more reliable on the high Schmidt number part.

### 4.3.2 Experimental results of the fixed-focus telescope

Lenses 1 and 2, as well as the PPKTP crystal have been placed at the theoretical positions, the very fine adjustment of the first focus size was done thanks to the fine tuning knob of the fiber output mount in the longitudinal direction - a very sensitive knob, as the fiber output beam is very divergent.

Whatever the deformations of the beam were, we have still measured actual precise positions of every lens for the fixed-focus telescope. The method to be sure to have the focus in the crystal was the make the beam have the same waist $15\ \mathrm{cm}$ in front of and $15\ \mathrm{cm}$ after the crystal. This would mean, for a Gaussian beam, that the focus is at the middle between this two points, i.e. in the center of the crystal.

In Figure 4.6 is given a table of the experimental results we had. Are given the positions of Lens 3 and Lens 4 with respect to the fiber output, the beam waist in the crystal, the beam waist $15\ \mathrm{cm}$ in front of or after (equal numbers from method used), and the theoretical number the latter waist should be, assuming Gaussian beam theory and a focus waist being the $w_\mathrm{p}$ measured.

In Figure 4.7 is given the experimental setup "manual", i.e. a curve given the positions you should set Lens 3 and Lens 4 for a wanted $w_\mathrm{p}$.

One can see that several points of the experimental data are obviously wrong. It is partly due to deformations which changed the curve, but also to the difficulty of collecting data : we used a Gaussian fit to know the size of the beams, method which brings majors failures whenever the beam is not Gaussian. But the trend of the position of the Lens 3 in function of the desired $w_\mathrm{p}$ is more or less the same, what leads us to hope that with less deformations, the fixed-focus telescope would work efficiently. The bigger variations on the position of the Lens 4 are due to beam aberrations, but also to the fact that its position is less sensitive, as it is a much weaker lens. Moving it from 5 mm often keeps the focus at less than a Rayleigh range of the crystal.

| Position L3 (cm) | Position L4 (cm) | wp (microns) | w(z=+- 15cm) (microns) | w(z=+- 15cm) theoretical value (microns) |
|---|---|---|---|---|
| 32 | 58.03 | 31 | 700 | 637 |
| 31.75 | 57.8 | 33 | 675 | 599 |
| 31.5 | 57.76 | 47 | 620 | 422 |
| 31.25 | 57.52 | 39 | 590 | 507 |
| 31 | 57.53 | 75 | 455 | 273 |
| 30.75 | 57.26 | 48 | 437 | 414 |
| 30.5 | 57.19 | 58 | 370 | 345 |
| 30.25 | 57.23 | 71 | 340 | 287 |
| 30 | 57.32 | 84 | 315 | 249 |
| 29.75 | 57.1 | 71 | 265 | 287 |
| 29.5 | 57.25 | 85 | 230 | 247 |
| 29.25 | 57.24 | 150 | 195 | 199 |
| 29.1 | 57.11 | 210 | 165 | 230 |

Figure 4.6: Experimental numbers of the fixed-focus telescope : positions of L3 and L4 with respect to the fiber output, beam waist in the crystal, beam waist $15$ cm in front of or after (equal numbers from method used), and the theoretical number the latter waist should be, assuming Gaussian beam theory and a focus waist being the $w_{\mathrm{p}}$ measured.

### 4.3.3 First experimental pictures of low Schmidt Number SPDC beam

In this section, we will give only the first pictures of the SPDC beam, in Figure 4.8. The pictures of both $w_{\mathrm{p}} = 31$ $\mu$m and $w_{\mathrm{p}} = 71.1$ $\mu$m under null and slightly negative phase mismatch have been shot with an Intensified CCD camera, with a gain of 100 and an integration time of 3s.

It is not the goal of this thesis to study them intensively, because, as written in 4.3.1, the setup will work much more properly on the biphoton setup table. But we can still guess that the structure is more compact for a tight focus regime, and the rings are thicker, what means that the ratio $\frac{w_{\mathrm{p}}}{w_{-}}$ is larger for tight foci -even if there is no factorization of the SPDC foreseen (Section 4.1 or [6]).

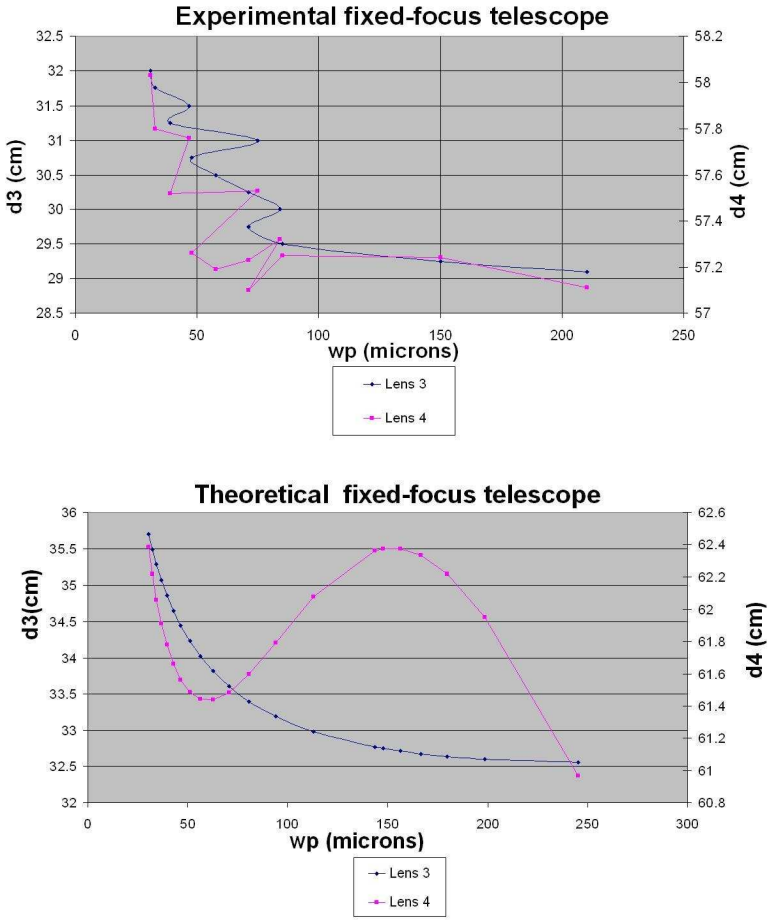


Figure 4.7: On the top is the experimental curve giving the position of Lens 3 and Lens 4 (origin being the output of the fiber) in function of the focussed beam waist in the crystal, on the bottom is the same curve but as computed by Maple

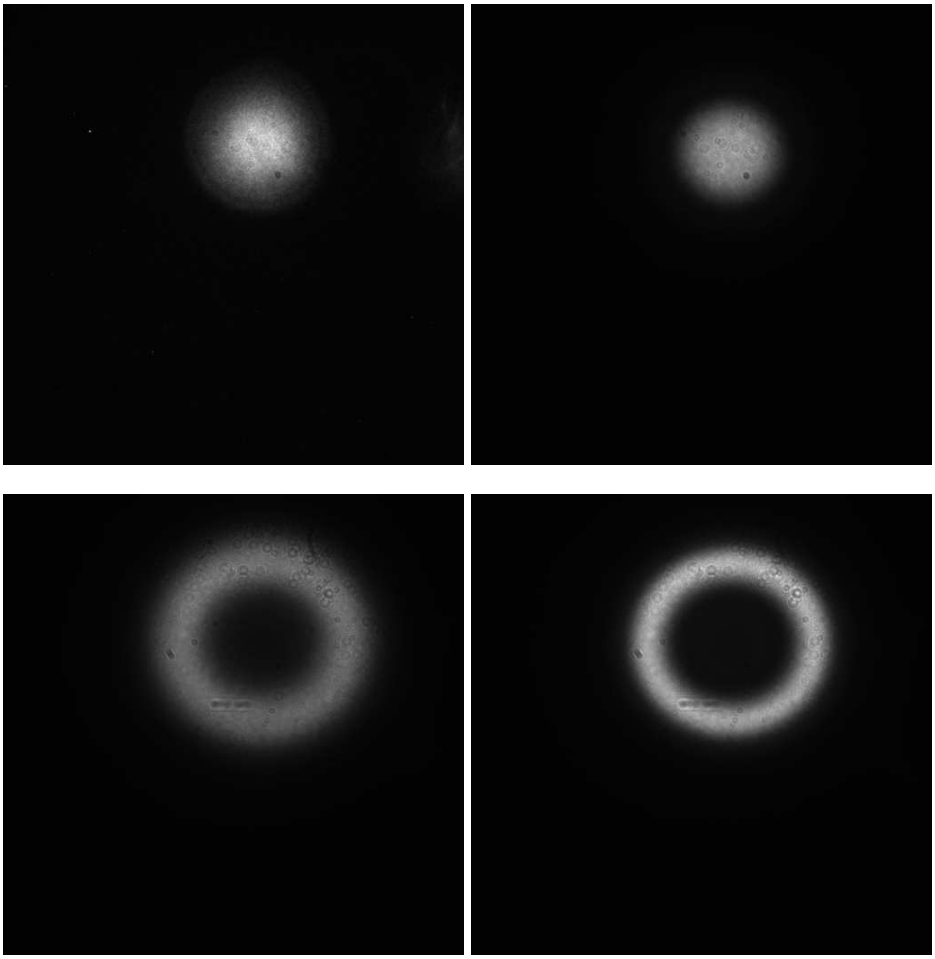

Figure 4.8: On the top are the pictures of the SPDC light under a null phase mismatch regime ($T = 60.4\,^{\circ}C$) for $w_{\mathrm{p}} = 31$ $\mu$m (left) and $w_{\mathrm{p}} = 71.1$ $\mu$m (right). On the bottom are the pictures for the same $w_{\mathrm{p}}$, at a slight negative phase mismatch ($T = 59.2\,^{\circ}C$)

# Chapter 5

# Conclusion

We have found out that there is no systematic trend in the results given by the calculation of the correlation matrix of the Quantum Efficiency or of the coincidence counts, at least for a $K \gg 1$ regime. We have also thought about how to calculate the correlation matrix, and showed that deepening the Quantum Efficiency pattern into a constant background (with the average of the Quantum Efficiency as value of the constant) lowers of around $10\%$ the size of the speckles, compared to calculating the correlation matrix with the bare Quantum Efficiency matrix. We have then presented the results we had for 70 scans, showing four times too low diff speckles size, using this strict measurement programme we have settled.

We have also given the reason why these diff speckles were a lot smaller than predicted by theory -the diffuser being within a Rayleigh range of the focus of the pump, but not at all of the phase matching profile, which is much more compact in the diffuser plane, so much more divergent. A little calculation gives the number of $5$ mm for the former distance between the diffuser and the focus. Now that we have made so that as this distance is less than a Rayleigh range of the phase-matching profile, the diff speckles have the size foreseen by theory.

We built a way to reduce the Schmidt Number of the experiment down to the minimum possible, which is taking place for $w_{\mathrm{p}} = 30\ \mu$m. We have showed than it is possible to build a setup that varies the size of the beam without moving the crystal, and this experimental setup has the same trend as the one we computed before. In more, when implemented on the biphoton setup, aberrations that spoiled the large foci regime should no more occur. We have showed four pictures of the two photon beam under this low K regime, and we can see, even with no extensive study of the subject (which we do not underestimate at all), that the structure is more compact and the rings are thicker.

# Chapter 6

# Further research

The first further research will be of course to go for an extensive study of the few excited modes two photon beam, and of the two photon speckles that go with. We are expecting that the two photon beam is no more separable into a sum of coordinates and a difference of coordinates parts. And, even if this factorization would still hold, as the pump is going down to $w_{\mathrm{p}} = 30$ $\mu$m, the sum speckles would have a comparable size to the former difference speckles we had -they were created with a width a the phase matching profile of $18$ $\mu$m. This mixing of sum and diff speckles would be enhanced by the fact that the two photon beam phase matching profile looks looser under the low K regime, as shown by thicker rings for $w_{\mathrm{p}} = 30$ $\mu$m.

Another orientation that one may bring is to average the speckles via a rotating diffuser.

# Bibliography


[1] J. W. Goodman, *Statistical Optics*, (1985).

[2] C. van Schooneveld, *Image Formation from Coherence Functions in Astronomy* (D. Reidel Publishing Company, ADDRESS, 1979).

[3] W. Tango and R. Q. Twiss, *Michelson Stellar Interferometry*, Progress in Optics **17**, 239 (1980).

[4] C. M. Waterman-Storer, A. Desai, C. Bulinski, and E. Salmon, *Fluorescent speckle microscopy, a method to visualize the dynamics of protein assemblies in living cells*, Current Biology **8**, 1227 (1980).

[5] J. J. D. Moerman, *Observation of Biphoton Speckles from Random Phase Plates*, Bachelor's thesis, Leiden University (2008).

[6] M. P. van Exter and W. Peeters, *Two-photon scattering random media*, Unpublished (2009).

[7] C. H. Monken, P. H. S. Ribeiro, and S. Pádua, *Transfer of angular spectrum and image formation in spontaneuous parametric down-conversion*, Physical Review A **57**, 3123 (1998).

[8] H. D. L. Pires and M. P. van Exter, *Observation of near-field correlations in spontaneous parametric down-conversion*, Physical Review A **79**, 041801 (2009).

[9] K. W. Chan, J. P. Torres, and J. H. Eberly, *Transverse entanglement migration in Hilbert space*, Physical Review A **75**, 050101 (2007).

[10] H. A. Haus, *Waves and Fields in Optoelectronics*, (1984).

[11] H. D. L. Pires, C. H. Monken, and M. P. van Exter, *Direct measurement of transverse mode entanglement in two-photon states*, Submitted (2009).

[12] C. Beenakker, J. Venderbos, and M. van Exter, *Two-photon speckle as a probe of multi-dimensional entanglement*, Physical Review Letters **102**, 193601 (2009).